Publishing Excellence Inspiring Progress
ARISTON PUBLICATIONS
MatSci Express
ISSN: 2997-8440 www.aristonpubs.com/matsci-express https://doi.org/10.69626/mse.2025.0356

RESEARCH ARTICLE

Porosity and Defect Modulation in Gamma–Irradiated Zinc Ferrite Nanoparticles for High Sensitivity Petrol Vapor Sensing

Siddheshwar D. Raut [1], Vishal V. Awasarmol [2], Sandip S. Pawar [3], Mahesh M. Hivrekar [4], Pravina P. Pawar [3], Shakuntala A. Shinde [1,*]

ABSTRACT: Zinc ferrite ($ZnFe_2O_4$) nanoparticle-based petrol vapor sensors were synthesized *via* a cost-effective sol–gel auto-combustion method and subsequently modified using γ-irradiation at doses of 2 and 5 kGy. The effect of γ-irradiation on the structural, morphological, and textural properties of $ZnFe_2O_4$ was systematically investigated, with particular emphasis on surface area and pore size distribution. Brunauer–Emmett–Teller (BET) analysis reveals a notable enhancement in specific surface area along with a substantial reduction in average pore size upon γ-irradiation, indicating the formation of a highly accessible mesoporous framework. Pelletized $ZnFe_2O_4$ sensors were evaluated toward petrol vapor at a concentration of 100 ppm under room-temperature operating conditions. The pristine $ZnFe_2O_4$ sensor exhibits a response of 23.43%, whereas the 2 and 5 kGy γ-irradiated sensors show significantly enhanced responses of 39.25% and 58.52%, respectively. The pronounced improvement in sensing performance is attributed to irradiation-induced defect states, increased density of active adsorption sites, and improved gas diffusion pathways resulting from optimized pore structure. The study demonstrates that γ-irradiation is an effective post-synthesis modification strategy for achieving highly sensitive, room-temperature petrol vapor sensors based on $ZnFe_2O_4$ nanoparticles, and the approach can be extended to other ferrite-based sensing materials.

Keywords: Gamma-irradiation, Petrol sensor, Zinc Ferrite ($ZnFe_2O_4$), Sol-gel auto-combustion.

Received: 25 September 2025; Revised: 27 October 2025; Accepted: 13 November 2025; Published Online: 03 December 2025

1. INTRODUCTION

The rapid growth of petroleum-based transportation and industrial activities has led to increased emission of volatile organic compounds (VOCs), among which petrol vapor is particularly hazardous due to its high flammability and adverse health effects [1]. Prolonged exposure to petrol vapor can cause respiratory disorders, neurological complications, and environmental pollution, necessitating the development of reliable gas sensors capable of detecting petrol vapor at low concentrations under ambient conditions [2-4]. Metal oxide semiconductor–based gas sensors have attracted extensive attention owing to their simplicity, low cost, and high sensitivity; however, achieving high sensing performance at room temperature remains a significant challenge [5, 6].

Spinel ferrites (MFe_2O_4, where M = Zn, Co, Ni, etc.) have emerged as promising sensing materials due to their structural stability, tunable electrical properties, and rich defect chemistry [7]. Among them, zinc ferrite ($ZnFe_2O_4$) is particularly attractive because of its chemical stability, environmentally benign nature, and semiconducting

[1] Sharadchandra Arts, Commerce and Science College, Naigaon, District Nanded-431709, Maharastra, India
[2] Swami Vivekanand Senior College, Mantha, District Jalna- 431504, Maharastra, India
[3] Dr. Babasaheb Ambedkar Marathwada University, Chh. Smabhajinagar-431004, Maharastra, India
[4] Gramin Technical and Management Campus, Vishnupuri, Nanded-431606, Maharastra, India

* Author to whom correspondence should be addressed: shakunshinde1973@gmail.com (Shakuntala A. Shinde)

© Ariston Publications 2025. All rights reserved.

behavior suitable for gas sensing applications [8-10]. Nevertheless, pristine $ZnFe_2O_4$ often suffers from limited surface area and insufficient active sites, resulting in modest sensing performance, especially at room temperature [11]. Therefore, effective strategies to tailor its surface properties and defect states are crucial for enhancing gas sensing efficiency [12].

Surface area enlargement, pore structure optimization, and defect engineering are widely recognized as key factors governing the gas sensing behavior of MOS-based sensors [13, 14]. A mesoporous architecture facilitates efficient gas diffusion, while surface defects such as oxygen vacancies and cation disorders act as active adsorption centers, enhancing surface reactions with target gas molecules. Conventional approaches such as elemental doping, composite formation, and morphological control have been explored to improve the sensing response of $ZnFe_2O_4$; however, these methods often involve complex synthesis steps or introduce secondary phases that may compromise material stability [15-17].

Gamma (γ) irradiation has recently gained attention as a clean and effective post-synthesis modification technique for tuning the structural and electronic properties of nanomaterials without altering their chemical composition [18]. High-energy γ-photons can induce lattice defects, modify surface states, and influence pore characteristics, thereby enhancing charge carrier transport and surface reactivity [19]. Raut *et al.* reported a simple and rapid sol–gel auto-combustion route for the synthesis of $ZnFe_2O_4$ nanoparticles and examined the influence of γ-irradiation at doses of 2 and 5 kGy on their chemiresistive gas sensing behavior. Pristine as well as γ-irradiated $ZnFe_2O_4$ nanoparticle pellet sensors were evaluated toward various target gases at room temperature. The study demonstrated that the 5 kGy γ-irradiated $ZnFe_2O_4$ sensor exhibited superior selectivity and enhanced response of 81% toward ammonia which is much better than the pristine (55%) and 2kGy (66%) gamma-irradiated samples, which was attributed to irradiation-induced enhancement in surface active sites, increased surface area, and modified pore characteristics [20]. Owing to its improved sensitivity, favorable response–recovery characteristics, and excellent stability, the γ-irradiated $ZnFe_2O_4$ material was identified as a promising low-cost candidate for high-performance room-temperature ammonia gas sensing applications [21]. Despite its proven effectiveness in tailoring functional properties of metal oxides, the application of γ-irradiation for improving the petrol vapor sensing performance of $ZnFe_2O_4$ nanoparticles remains largely unexplored.

In this work, $ZnFe_2O_4$ nanoparticles were synthesized using a sol–gel auto-combustion method and subsequently subjected to γ-irradiation at doses of 2 and 5 kGy to modulate their porosity and defect structure. The influence of γ-irradiation on structural, morphological, and textural properties was systematically investigated, with particular emphasis on surface area and pore size distribution. The gas sensing performance of pelletized $ZnFe_2O_4$ sensors toward petrol vapor was evaluated at room temperature, and the role of irradiation-induced defects and mesoporosity in enhancing sensing response was critically analyzed. This study highlights γ-irradiation as an effective post-synthesis strategy for developing high-performance, room-temperature ferrite-based gas sensors.

2. EXPERIMENTAL DETAILS

2.1. Preparation of $ZnFe_2O_4$ Nanoparticles

Zinc ferrite ($ZnFe_2O_4$) nanoparticles were synthesized *via* a sol–gel auto-combustion route using zinc nitrate hexahydrate [$Zn(NO_3)_2 \cdot 6H_2O$] and ferric nitrate nonahydrate [$Fe(NO_3)_3 \cdot 9H_2O$] as metal precursors. Citric acid monohydrate ($C_6H_8O_7 \cdot H_2O$) was employed as a complexing agent and fuel to facilitate homogeneous chelation of metal ions and to suppress premature hydroxide precipitation. The precursors were dissolved in deionized water in stoichiometric proportions under continuous stirring. The pH of the resulting solution was adjusted to neutral (~7) by the controlled addition of liquid ammonia. The homogeneous mixture was heated at 80–90 °C under magnetic stirring for about ~2 h until it transformed into a viscous gel. Continued heating led to spontaneous auto-combustion of the dried gel, yielding a voluminous, porous ash. The obtained precursor powder was calcined at 500 °C for 5 h to achieve phase formation and improve crystallinity. After calcination, the powder was finely ground using an agate mortar and pestle to obtain uniform $ZnFe_2O_4$ nanoparticles. For gas sensing studies, pellet-shaped sensors were fabricated by pressing ~1 g of $ZnFe_2O_4$ nanopowder using an automatic hydraulic press under the pressure of 7 tons. The resulting pellets possessed a thickness of ~0.3 cm and a diameter of ~1 cm. To enhance mechanical stability and interparticle connectivity, the pellets were thermally treated at 250 °C for 2 h prior to irradiation and sensing measurements.

2.2. Gamma Irradiation Treatment

Post-synthesis modification of the $ZnFe_2O_4$ nanopellets was carried out through γ-irradiation at the Department of Biophysics, Government Institute of Science, Aurangabad, Maharashtra, India. A Gamma Chamber-900 facility equipped with a cobalt-60 (^{60}Co) radioactive source was used to deliver high-energy γ-rays at a dose rate of approximately 72 Gy h^{-1}. The pellets were exposed to total irradiation doses of 2 kGy and 5 kGy under ambient atmospheric conditions.

2.3. Material Characterization

The crystalline structure and phase evolution of pristine and γ-irradiated $ZnFe_2O_4$ nanopellets were examined using X-ray diffraction (XRD) (Bruker D8 Discover diffractometer). Surface morphology was analyzed using scanning electron microscopy (SEM, Hitachi S-4800). The textural properties,

© Ariston Publications 2025. All rights reserved.

including specific surface area and pore size distribution, were evaluated through N_2 adsorption–desorption measurements using a Micromeritics ASAP 2010 analyzer. The Brunauer–Emmett–Teller (BET) method was employed to calculate surface area, while pore size distribution was determined from the desorption curve of the isotherms.

2.4. Gas Sensing Measurements

The petrol vapor sensing characteristics of pristine and γ-irradiated $ZnFe_2O_4$ nanopellet sensors were investigated using a static gas sensing system operated at room temperature. The sensing measurements were carried out in a sealed glass chamber with an effective volume of 250 mL under ambient atmospheric conditions.

To establish electrical contacts, two parallel silver electrodes were coated on the top surface of each $ZnFe_2O_4$ pellet using conducting silver paste. The prepared pellets (pristine, 2 kGy, and 5 kGy γ-irradiated) were individually placed inside the sensing chamber and allowed to stabilize in air prior to exposure to petrol vapor.

The desired vapor concentration (100 ppm) was calculated based on the chamber volume, liquid density, molecular weight, and testing temperature. Upon injection of petrol vapor, the change in the resistance of the $ZnFe_2O_4$ sensors was continuously recorded using a computer-interfaced Keithley 6514 electrometer.

The sensing response was calculated using the formula [21]:

$$S\ (\%) = \frac{R_a - R_g}{R_a} \times\ 100 \qquad (1)$$

Where, R_a is resistance of the sensor in air, R_g is resistance of the sensor in presence of petrol vapor.

After completion of each sensing cycle, the chamber was purged with fresh air by opening the outlet valve, allowing the sensor to recover to its baseline resistance. The response–recovery behavior, repeatability, concentration-dependent response, and long-term stability of the sensors were systematically evaluated to assess their sensing performance and operational reliability.

3. RESULTS AND DISCUSSION

3.1. Structural and morphological analysis

The crystalline structure of $ZnFe_2O_4$ nanoparticles was confirmed by XRD analysis (Figure 1), which shows a well-defined cubic spinel phase for pristine as well as γ-irradiated samples (2 and 5 kGy). All diffraction peaks matched closely with the standard JCPDS card no. 22–1012, indicating phase purity and structural stability of $ZnFe_2O_4$ under γ-irradiation. Although no additional phases were detected after irradiation, a gradual reduction in the intensity of selected reflections, particularly the (222) plane, was observed with increasing γ-dose. This behavior suggests irradiation-induced lattice distortions and defect formation, which are commonly associated with pore generation and enhanced surface reactivity-key factors for gas sensing applications.

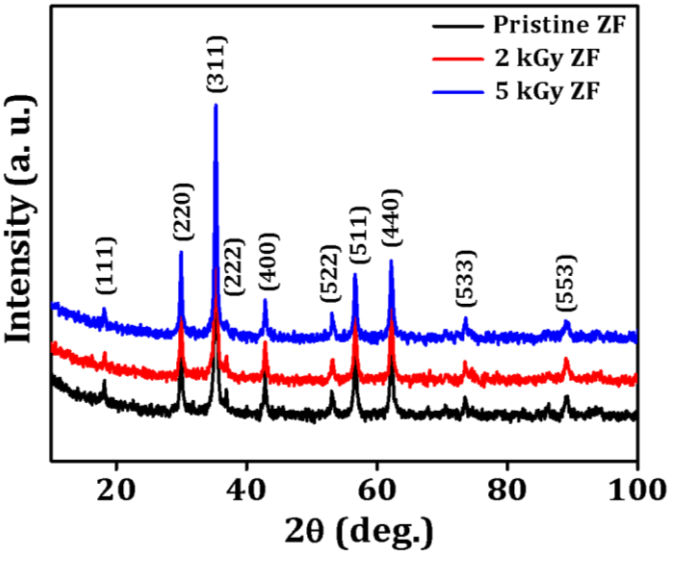


Fig. 1. XRD graphs of pristine, 2 kGy, and 5 kGy γ-irradiated $ZnFe_2O_4$ nanoparticles.

The surface morphology of pristine and γ-irradiated $ZnFe_2O_4$ pellet sensors was examined using FE-SEM, as shown in Figure 2 (a–c). All samples exhibit a compact assembly of nanoparticles with irregular shapes and moderate agglomeration. The surfaces are neither highly rough nor well-faceted, which makes precise identification of individual crystallite boundaries challenging. A few nanoparticles coalesce to form larger island-like structures, while inter-particle crevices and voids are clearly visible throughout the sensing surface. These interstitial gaps can act as active channels for gas diffusion and adsorption, thereby contributing positively to sensing performance. Notably, γ-irradiation does not induce any drastic morphological transformation, indicating that the enhancement in gas response originates primarily from microstructural modifications and defect generation rather than from large-scale morphological changes [22]. High-resolution TEM analysis (Figure 2(d)) further supports the XRD findings by confirming the crystalline nature of $ZnFe_2O_4$ nanoparticles. The observed lattice fringes with an interplanar spacing of approximately 0.25 nm correspond to the (311) plane of cubic spinel $ZnFe_2O_4$, validating the preservation of crystal structure at the nanoscale even after γ-irradiation.

3.2. Surface area and pore structure analysis

The N_2 adsorption–desorption curves of pristine and γ-irradiated $ZnFe_2O_4$ nanoparticle pellet sensors (Figure 3) exhibit type-IV behavior with pronounced hysteresis loops at

© Ariston Publications 2025. All rights reserved.

higher relative pressures, confirming their mesoporous nature. γ-irradiation results in a systematic increase in specific surface area, with the 2 and 5 kGy samples showing higher values than the pristine $ZnFe_2O_4$, which is attributed to irradiation-induced grain refinement and defect generation. Concurrently, the average pore diameter decreases significantly after irradiation, shifting the pore distribution toward smaller mesopores, as shown in the inset of Figure 3.

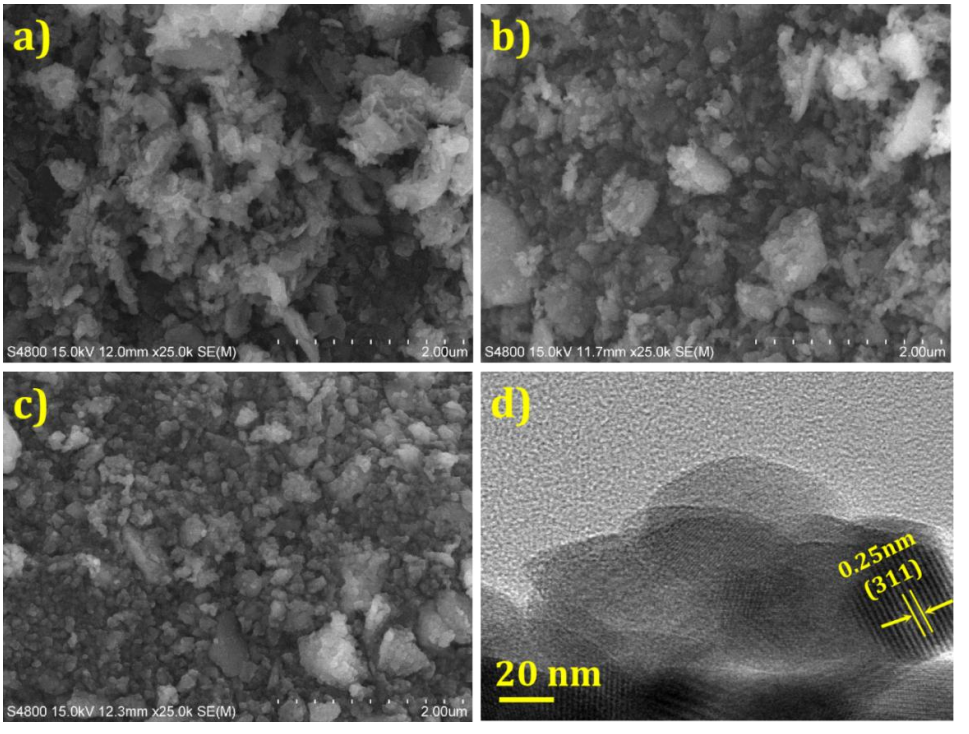
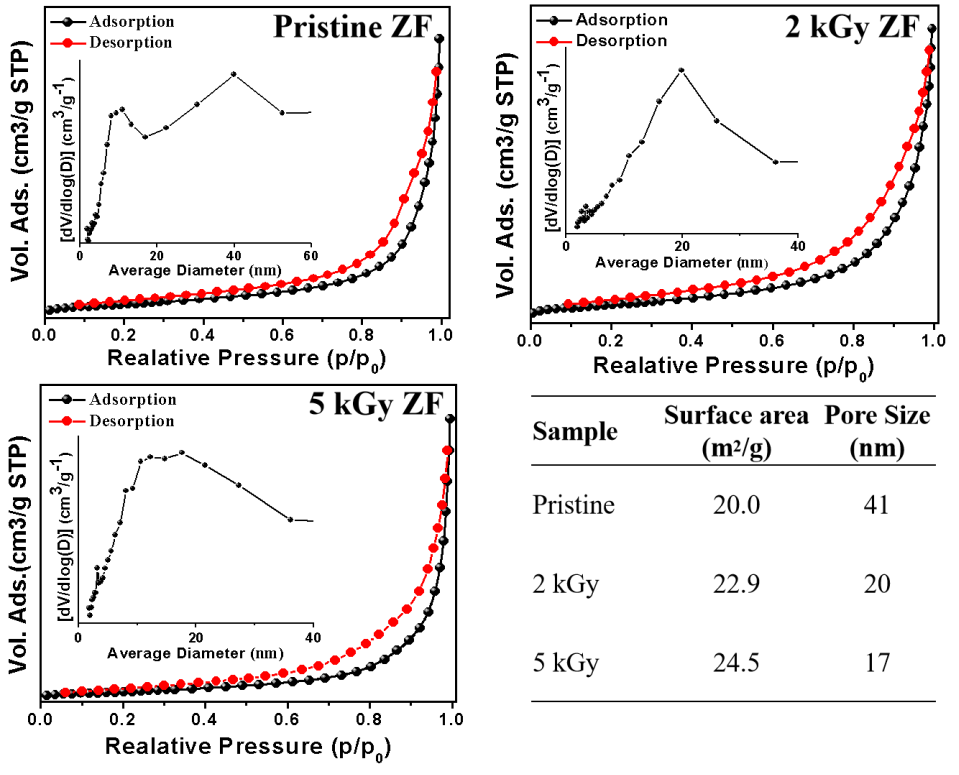


Fig. 2. FESEM images of; (a) pristine, (b) 2 kGy, (c) 5 kGy γ-irradiated $ZnFe_2O_4$ nanoparticles, and (d) HRTEM image showing lattice fringes with a d-spacing of the γ-irradiated $ZnFe_2O_4$ nanoparticles.



Sample	Surface area (m^2/g)	Pore Size (nm)
Pristine	20.0	41
2 kGy	22.9	20
5 kGy	24.5	17

Fig. 3. N_2 adsorption–desorption isotherms and pore-size distribution of; (a) pristine, (b) 2 kGy, and (c) 5 kGy γ-irradiated $ZnFe_2O_4$ NP-pellet sensors (inset of each shows respective pore-size distribution measurement), and (d) mesoporous nature with enhanced surface area after irradiation.

© Ariston Publications 2025. All rights reserved.

The modified surface area with corresponding pore size is shown in Figure 3(d). This pore narrowing enhances the accessible internal surface and improves gas diffusion and adsorption efficiency. The combined increase in surface area and optimized mesoporosity facilitates stronger interaction between petrol vapor molecules and the $ZnFe_2O_4$ surface, thereby contributing to the enhanced sensing response observed for the γ-irradiated sensors [23].

3.2. Gas-sensing results toward petrol vapor

The petrol vapor sensing performance of pristine and γ-irradiated $ZnFe_2O_4$ nanoparticle pellet sensors was systematically investigated @room temperature (300 K) using 100 ppm petrol vapor as the target gas. Figure 4 illustrate the dynamic response–recovery characteristics, concentration-dependent behavior, repeatability, and long-term durability of the sensors. The pristine $ZnFe_2O_4$ sensor exhibits a moderate response of 23.43%, whereas γ-irradiated samples show a pronounced enhancement, with responses increasing to 39.25% for 2 kGy and 58.52% for 5 kGy irradiated sensors. This clear improvement confirms the beneficial role of γ-irradiation in activating the sensing surface.

The γ-irradiated sensors, especially the 5 kGy sample, shows higher response but comparatively slower response and recovery behavior, which can be attributed to the increased surface area and modified pore network that require longer diffusion and equilibration times for petrol vapor molecules. Concentration-dependent measurements reveal a systematic increase in sensor response with increasing petrol vapor concentration, confirming effective surface-controlled sensing behavior and good sensitivity in the investigated concentration range.

Repeatability studies over multiple cycles show nearly identical response magnitudes with negligible baseline drift, highlighting excellent chemical stability and reversibility of the $ZnFe_2O_4$ sensors. Furthermore, durability measurements carried out over an extended period demonstrate minimal degradation in sensing response, confirming the robustness of the pelletized $ZnFe_2O_4$ sensors under ambient operating conditions.

The enhanced petrol vapor sensing performance of γ-irradiated $ZnFe_2O_4$ sensors is attributed to irradiation-induced defect states, such as oxygen vacancies and surface dangling bonds, which increase the density of active adsorption sites. In addition, BET analysis confirms that γ-irradiation leads to increased surface area and reduced pore size, resulting in a highly accessible mesoporous framework that facilitates efficient gas diffusion and surface reactions. Upon exposure to petrol vapor (a reducing gas), the interaction with chemisorbed oxygen species releases trapped electrons back into the conduction band of $ZnFe_2O_4$, leading to a measurable change in resistance. The synergistic effect of enhanced surface reactivity, optimized porosity, and defect-mediated charge transport accounts for the superior sensing performance of γ-irradiated $ZnFe_2O_4$ sensors.

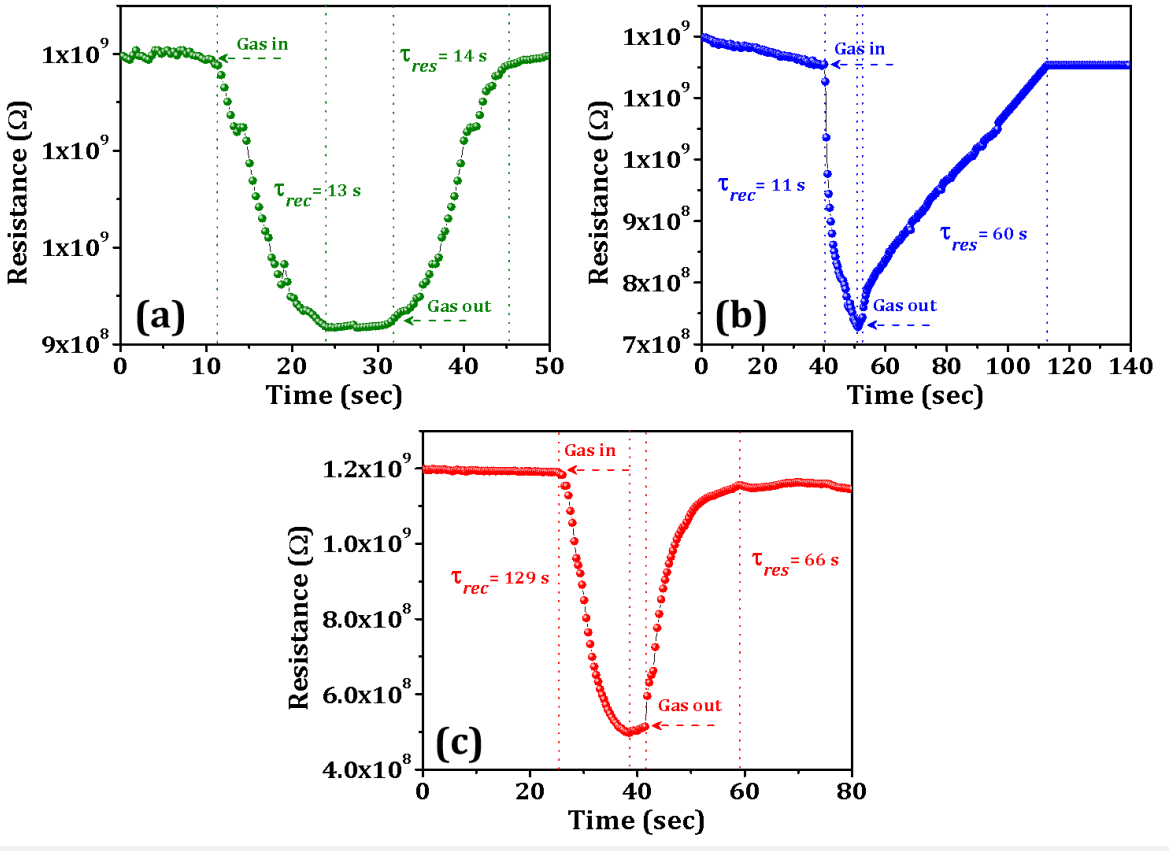


Fig. 4. Gas sensing response–recovery plots of; (a) pristine, (b) 2 kGy, and (c) 5 kGy γ-irradiated $ZnFe_2O_4$ NP-pellet petrol vapor sensors.

© Ariston Publications 2025. All rights reserved.

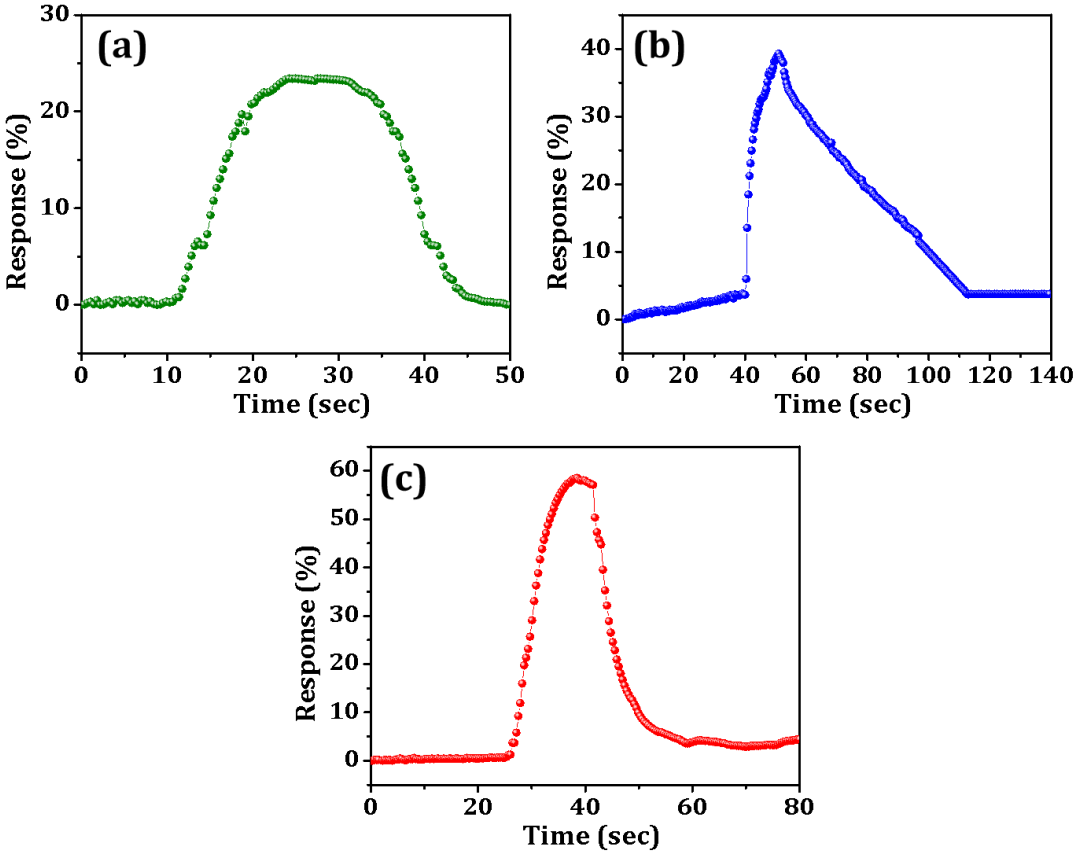


Fig. 5. Response *vs.* time plots of; (a) Pristine, (b) 2kGy, and (c) 5kGy $ZnFe_2O_4$ NP-pellet petrol sensors.

The response–time transients (Figure 5) illustrate the dynamic sensing characteristics of pristine and γ-irradiated $ZnFe_2O_4$ sensors toward petrol vapor at room temperature (Figure 5). Upon gas exposure, all sensors show a rapid change in resistance, followed by saturation, confirming effective interaction between petrol molecules and the sensor surface. Compared to the pristine sample, the γ-irradiated sensors exhibit a steeper response profile and higher peak response, indicating faster surface reaction kinetics and improved charge transfer arising from irradiation-induced defect states and optimized porosity. During gas removal, the resistance gradually returns toward the baseline, demonstrating good recovery behavior governed by desorption of petrol species. The slight variation in response and recovery slopes among the samples reflects differences in pore accessibility and defect density, with higher γ-dose leading to enhanced sensitivity but relatively slower relaxation due to stronger adsorption at abundant active sites.

The repeatability of the $ZnFe_2O_4$-based sensor was evaluated by exposing it to successive cycles of petrol vapor at room temperature, as shown in the Figure 6. The sensor exhibits nearly identical response amplitudes and stable baseline recovery over multiple cycles, indicating excellent reproducibility and reversibility of the sensing process. The absence of noticeable signal drift or degradation confirms the chemical stability of the sensing material and the robustness of adsorption–desorption dynamics, demonstrating the sensor's reliable performance for repeated petrol vapor detection.

The dynamic response curves recorded at different petrol vapor concentrations demonstrate a clear concentration-dependent sensing behavior for pristine and γ-irradiated $ZnFe_2O_4$ sensors (Figure 7). As the petrol concentration increases, the sensor response rises progressively, indicating enhanced adsorption and oxidation of petrol molecules on the sensor surface and a corresponding increase in charge carrier modulation. Among all samples, the γ-irradiated sensors exhibit higher response amplitudes across the entire concentration range, with the 5 kGy–treated $ZnFe_2O_4$ showing the most pronounced response, reflecting its higher density of irradiation-induced defects and improved mesoporous accessibility. At higher concentrations, the tendency toward response saturation suggests partial occupation of available active sites and limited diffusion through the sensing layer. Overall, the monotonic increase in response with concentration confirms reliable sensing characteristics, good sensitivity, and effective surface reaction kinetics of γ-irradiated $ZnFe_2O_4$ toward petrol vapor at room temperature.

The durability characteristics (Figure 8) of pristine and γ-irradiated $ZnFe_2O_4$ sensors were evaluated by monitoring their response to petrol vapor over an extended period. As shown in the figure, all sensors exhibit nearly constant response values with negligible fluctuation throughout the testing duration, indicating excellent signal stability.

© Ariston Publications 2025. All rights reserved.

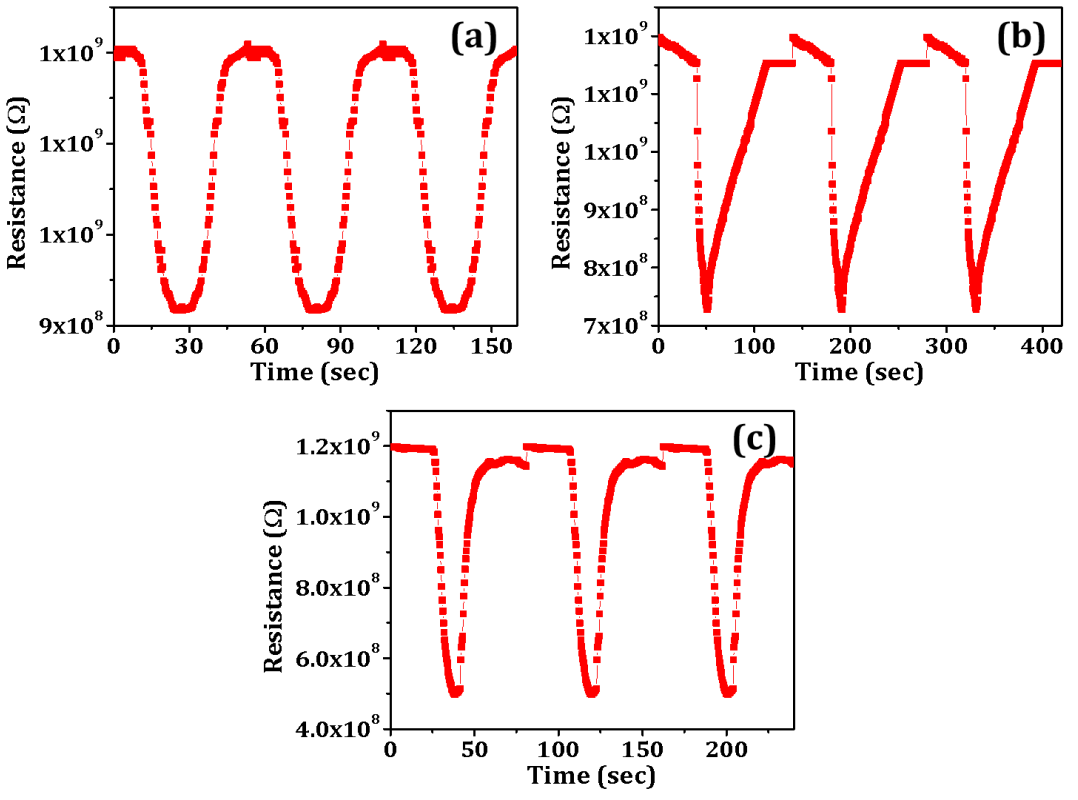


Fig. 6. Repeatability curves of; (a) Pristine, (b) 2kGy, and (c) 5kGy $ZnFe_2O_4$ NP-pellet sensors at 100 ppm concentration.

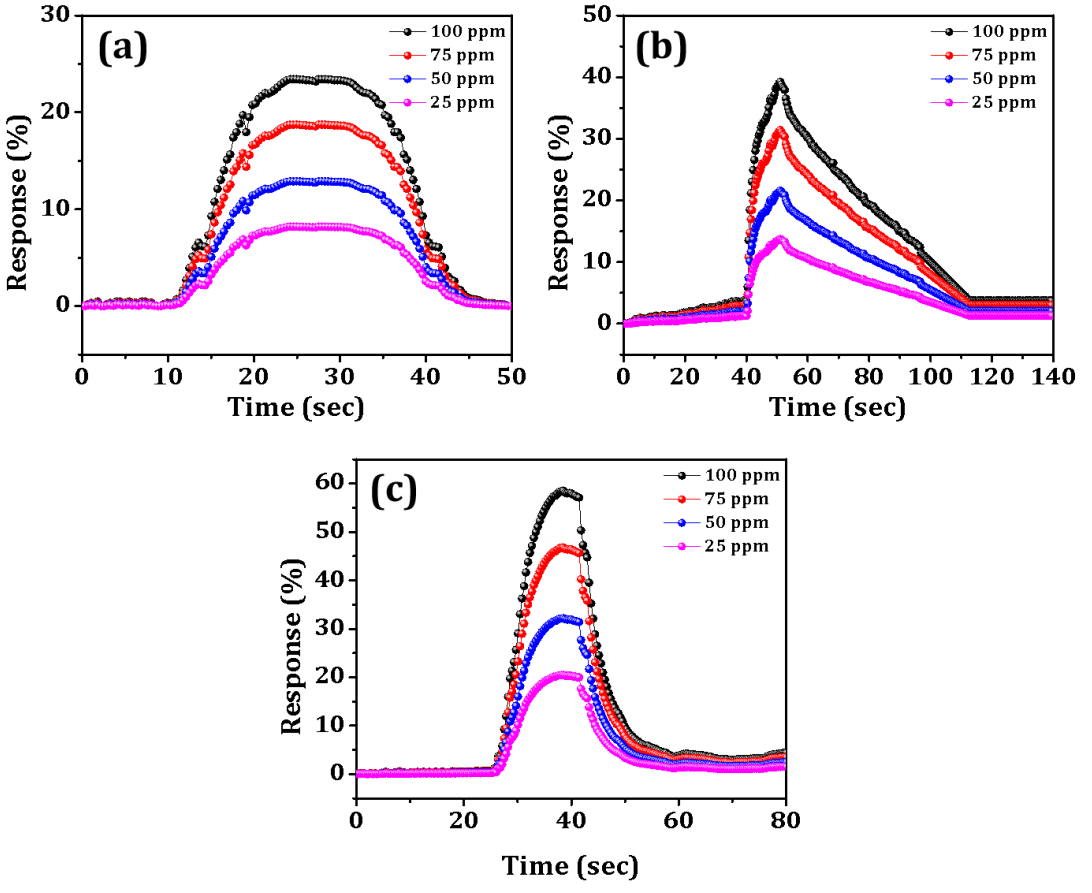


Fig. 7. The concentration effect on the sensing response of; (a) Pristine, (b) 2 kGy, and (c) 5 kGy γ-irradiated $ZnFe_2O_4$ NP-pellet sensors.

© Ariston Publications 2025. All rights reserved.

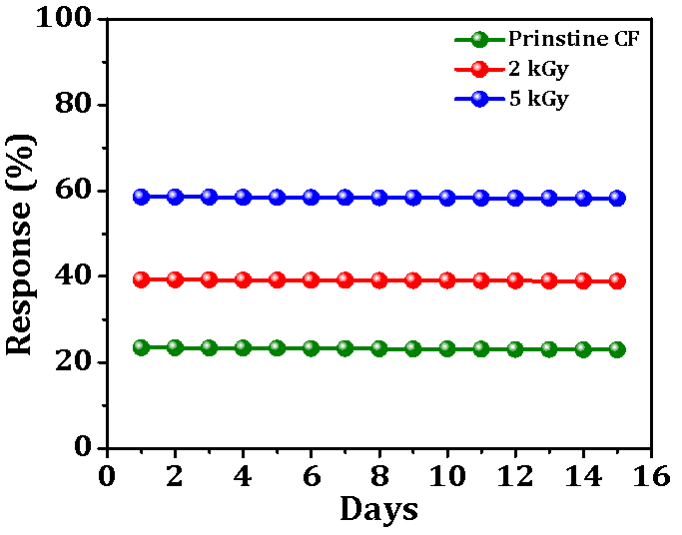


Fig. 8. Long-term stability of pristine and γ-irradiated $ZnFe_2O_4$ NP-pellet sensors.

Notably, the γ-irradiated sensors, particularly the 5 kGy–treated $ZnFe_2O_4$, maintain a consistently higher response compared to the pristine sample without any noticeable degradation. This stable performance confirms that γ-irradiation does not compromise the structural or chemical integrity of $ZnFe_2O_4$; instead, the irradiation-induced defect states and optimized porosity remain robust during prolonged operation. The observed durability highlights the suitability of γ-irradiated $ZnFe_2O_4$ sensors for reliable, long-term room-temperature petrol vapor sensing applications.

4. CONCLUSION

$ZnFe_2O_4$ nanoparticle-based petrol vapor sensors were successfully developed using a cost-effective sol–gel auto-combustion route, and their sensing characteristics were systematically tuned through γ-irradiation at doses of 2 and 5 kGy. γ-irradiation significantly modified the textural properties of $ZnFe_2O_4$, as evidenced by BET analysis showing an increase in specific surface area and a marked reduction in average pore size, leading to a highly accessible mesoporous structure. These irradiation-induced modifications translated directly into enhanced petrol vapor sensing performance at room temperature, with the sensor response improving from 23.43% for pristine $ZnFe_2O_4$ to 39.25% and 58.52% for the 2 and 5 kGy γ-irradiated sensors, respectively, at 100 ppm petrol vapor concentration. The improved sensing behavior is attributed to the generation of irradiation-induced defect states, a higher density of active adsorption sites, and more efficient gas diffusion pathways within the optimized porous network. In addition, the γ-irradiated sensors exhibited stable, repeatable, and durable sensing responses, highlighting their robustness for practical applications. Overall, this study establishes γ-irradiation as a simple and effective post-synthesis strategy for enhancing the room-temperature petrol vapor sensing performance of $ZnFe_2O_4$ nanoparticles and suggests its broader applicability for tailoring the functional properties of other ferrite-based gas sensing materials.

DECLARATIONS

Ethical Approval

We affirm that this manuscript is an original work, has not been previously published, and is not currently under consideration for publication in any other journal or conference proceedings. All authors have reviewed and approved the manuscript, and the order of authorship has been mutually agreed upon.

Funding

Not applicable

Availability of data and material

All of the data obtained or analyzed during this study is included in this paper.

Conflicts of Interest

The authors declare that they have no financial or personal interests that could have influenced the research and findings presented in this paper. The authors alone are responsible for the content and writing of this article.

Author's contribution statement

Authors contributed equally to this work.

REFERENCES

[1] Singh, B.P., Singh, M., Ulman, Y., Sharma, U., Pradhan, R., Sahoo, J., Padhi, S., Chandra, P., Koul, M., Tripathi, P.N. and Kumar, D., **2023**. Distribution and temporal variation of total volatile organic compounds concentrations associated with health risk in Punjab, India. *Case Studies in Chemical and Environmental Engineering*, 8, 100417. https://doi.org/10.1016/j.cscee.2023.100417.

[2] Saxena, P. and Shukla, P., **2023**. A review on recent developments and advances in environmental gas sensors to monitor toxic gas pollutants. *Environmental*

© Ariston Publications 2025. All rights reserved.

Progress & Sustainable Energy, 42(5), e14126. https://doi.org/10.1002/ep.14126.

[3] Tumberphale, U.B., Jadhav, S.S., Raut, S.D., Shinde, P.V., Sangle, S., Shaikh, S.F., Al-Enizi, A.M., Ubaidullah, M., Mane, R.S. and Gore, S.K., **2020**. Tailoring ammonia gas sensing performance of La^{3+}-doped copper cadmium ferrite nanostructures. *Solid State Sciences*, 100, 106089. https://doi.org/10.1016/j.solidstatesciences.2019.106089.

[4] Butt, M.A. and Piramidowicz, R., **2024**. Integrated photonic sensors for the detection of toxic gasses—A review. *Chemosensors*, 12(7), 143. https://doi.org/10.3390/chemosensors12070143.

[5] Zhang, J., Qin, Z., Zeng, D. and Xie, C., **2017**. Metal-oxide-semiconductor based gas sensors: screening, preparation, and integration. *Physical Chemistry Chemical Physics*, 19(9), 6313-6329. https://doi.org/10.1039/C6CP07799D

[6] Goel, N., Kunal, K., Kushwaha, A. and Kumar, M., **2023**. Metal oxide semiconductors for gas sensing. *Engineering Reports*, 5(6), e12604. https://doi.org/10.1002/eng2.12604.

[7] Dippong, T., Levei, E.A. and Cadar, O., **2021**. Recent advances in synthesis and applications of MFe_2O_4 (M= Co, Cu, Mn, Ni, Zn) nanoparticles. *Nanomaterials*, 11(6), 1560. https://doi.org/10.1002/eng2.12604.

[8] Mugutkar, A.B., Gore, S.K., Patange, S.M., Mane, R.S., Raut, S.D., Shaikh, S.F., Ubaidullah, M., Pandit, B. and Jadhav, S.S., **2022**. Ammonia gas sensing and magnetic permeability of enhanced surface area and high porosity lanthanum substituted Co–Zn nano ferrites. *Ceramics International*, 48(11), 15043-15055. https://doi.org/10.1016/j.ceramint.2022.02.033.

[9] Nemufulwi, M.I., Swart, H.C. and Mhlongo, G.H., **2023**. Advances of nano-enabled $ZnFe_2O_4$ based-gas sensors for VOC detection and their potential applications: a review. *Processes*, 11(11), 3122. https://doi.org/10.3390/pr11113122.

[10] Abdulhamid, Z.M., Dabbawala, A.A., Delclos, T., Straubinger, R., Rueping, M., Polychronopoulou, K. and Anjum, D.H., **2023**. Synthesis, characterization, and preliminary insights of $ZnFe_2O_4$ nanoparticles into potential applications, with a focus on gas sensing. *Scientific Reports*, 13(1), 19705. https://doi.org/10.1038/s41598-023-46960-w.

[11] Ye, M., Yang, C., Sun, Y., Wang, J., Wang, D., Zhao, Y., Zhu, Z., Liu, P., Zhu, J., Li, C. and Peng, W., **2022**. $ZnFe_2O_4$/graphitic carbon nitride nano/microcomposites for the enhanced electrochemical sensing of H_2O_2. *ACS Applied Nano Materials*, 5(8), 10922-10932. https://doi.org/10.1021/acsanm.2c02204.

[12] Sangale, S.S., Jadhav, V.V., Shaikh, S.F., Shinde, P.V., Ghule, B.G., Raut, S.D., Tamboli, M.S., Al-Enizi, A.M. and Mane, R.S., **2020**. Facile one-step hydrothermal synthesis and room-temperature NO2 sensing application of α-Fe_2O_3 sensor. *Materials Chemistry and Physics*, 246, 122799. https://doi.org/10.1016/j.matchemphys.2020.122799.

[13] Nadargi, D.Y., Umar, A., Nadargi, J.D., Lokare, S.A., Akbar, S., Mulla, I.S., Suryavanshi, S.S., Bhandari, N.L. and Chaskar, M.G., **2023**. Gas sensors and factors influencing sensing mechanism with a special focus on MOS sensors. *Journal of Materials Science*, 58(2), pp.559-582. https://doi.org/10.1007/s10853-022-08072-0.

[14] Mugutkar, A.B., Gore, S.K., Raut, S.D., Patange, S.M., Mane, R.S., Shaikh, S.F., Shirsath, S.E. and Jadhav, S.S., **2025**. Room-temperature acetone gas sensing using Sm-doped Co–Zn ferrite nanoparticles: role of mesoporosity and oxygen vacancies in enhancing sensor response. *Nanoscale Advances*, 7(22), 7259-7272. https://doi.org/10.1039/D5NA00631G.

[15] Yang, X., Deng, Y., Yang, H., Liao, Y., Cheng, X., Zou, Y., Wu, L. and Deng, Y., **2023**. Functionalization of mesoporous semiconductor metal oxides for gas sensing: Recent advances and emerging challenges. *Advanced Science*, 10(1), 2204810. https://doi.org/10.1002/advs.202204810.

[16] Hu, S., Li, C., Li, K., Teng, W., Li, F., Zhang, P. and Wang, H., **2024**. Advanced mesoporous adsorbents and catalysts for CO_2, NO_x, and VOC removal: mechanisms and applications. *Environmental Science: Nano*, 11(12), 4666-4691. https://doi.org/10.1039/D4EN00621F.

[17] de AA. Soler-Illia, G.J., Sanchez, C., Lebeau, B. and Patarin, J., **2002**. Chemical strategies to design textured materials: from microporous and mesoporous oxides to nanonetworks and hierarchical structures. *Chemical Reviews*, 102(11), 4093-4138. https://doi.org/10.1021/cr0200062.

[18] Huang, S., Yue, C., Uvdal, K. and Hu, Z., **2025**. Recent advances in irradiation-mediated synthesis and tailoring of inorganic nanomaterials for photo-/electrocatalysis. *Nanoscale Advances*, 7, 384-418. https://doi.org/10.1039/D4NA00806E.

 © Ariston Publications 2025. All rights reserved.

[19] Alhindawy, I.G. and Mahmoud, K.A., **2025**. Engineered zirconia nanomaterials for circular environmental and nuclear applications: dual-function design for photocatalytic pollutant degradation and gamma-ray shielding. *Advanced Composites and Hybrid Materials*, 8(4), 317. https://doi.org/10.1007/s42114-025-01379-x.

[20] Raut, S.D., Awasarmol, V.V., Ghule, B.G., Shaikh, S.F., Gore, S.K., Sharma, R.P., Pawar, P.P. and Mane, R.S., **2018**. γ-irradiation induced zinc ferrites and their enhanced room-temperature ammonia gas sensing properties. *Materials Research Express*, 5(3), 035702. https://doi.org/10.1088/2053-1591/aab3eb.

[21] Raut, S.D., Awasarmol, V.V., Ghule, B.G., Shaikh, S.F., Gore, S.K., Sharma, R.P., Pawar, P.P. and Mane, R.S., **2018**. Enhancement in room-temperature ammonia sensor activity of size-reduced cobalt ferrite nanoparticles on γ-irradiation. *Materials Research Express*, 5(6), 065035. https://doi.org/10.1088/20531591/aac99d.

[22] Chowdhury, N.K. and Bhowmik, B., **2021**. Micro/nanostructured gas sensors: the physics behind the nanostructure growth, sensing and selectivity mechanisms. *Nanoscale Advances*, 3(1), 73-93. https://doi.org/10.1039/D0NA00552E.

[23] Nemufulwi, M.I., Swart, H.C. and Mhlongo, G.H., **2023**. Advances of nano-enabled $ZnFe_2O_4$ based-gas sensors for VOC detection and their potential applications: a review. *Processes*, 11(11), 3122. https://doi.org/10.3390/pr11113122.

© Ariston Publications 2025. All rights reserved.